Ferrimagnetic $Mn_4N(111)$ layers grown on 6H-SiC(0001) and GaN(0001) by reactive molecular-beam epitaxy

S. Dhar,[a] O. Brandt, and K. H. Ploog
Paul-Drude-Institut für Festkörperelektronik, Hausvogteiplatz 5-7, D-10117 Berlin, Germany

(Received 15 November 2004; accepted 27 January 2005; published online 8 March 2005)

Epitaxial films of ferrimagnetic $Mn_4N(111)$ are grown directly on 6H-SiC(0001) substrates and GaN/6H-SiC(0001) templates using reactive molecular-beam epitaxy. The films are free from secondary phases and exhibit the theoretical saturation magnetization of Mn_4N.
 [DOI: 10.1063/1.1884748]

Epitaxial growth of ferromagnetic thin films on semiconductors is currently attracting much interest, since these structures have the potential for future spintronics applications. Various metallic ferromagnetic layers such as MnGa, MnAs, and Fe on semiconductors such as GaAs and Si have been investigated,[1–3] including metallic-ferromagnet/semiconductor multilayer structures.[4–6] However, no such investigations have been reported for wide-bandgap semiconductors such as SiC and GaN, although these materials are prime candidates for future electronic and optoelectronic devices.

In this respect, manganese nitride (Mn-N) is a naturally appealing candidate. Mn-N is known to exist in several bulk phases,[7] and most of these phases are antiferromagnetic in nature, with the singular exception of Mn_4N (the ε phase), which is a ferrimagnetic metal with a Néel temperature (T_N) as high as 738 K.[8–10] Another motivation to study Mn_4N is to understand the unknown inclusions, which cause ferromagnetism in (Ga,Mn)N.[11] However, this phase has scarcely been investigated so far, since it has proven to be difficult to be synthesized. Recently, the interest in Mn_4N has revived, and Ching *et al.*[12] and Yang *et al.*[13] have attempted the growth of Mn_4N on Si(001) and MgO(001) substrates, respectively. However, in either case the deposits were mixtures of the various Mn-N phases,[13] or were even contaminated by Mn-O phases.[12]

The crystal structure of Mn_4N belongs to the space group $P\bar{4}3m$, and is most simply described by the intersection of a fcc Mn sublattice at the origin (000) and a simple cubic lattice of N atoms in body-centered position $(\frac{1}{2}\frac{1}{2}\frac{1}{2})$.[9,10] The {111}-planes of Mn_4N exhibit a trigonal symmetry, basically matching the hexagonal symmetry of the *c*-plane (0001) of SiC or GaN, the commonly used plane for the epitaxial growth of these semiconductors. However, the lattice mismatch of ≈11% with respect to 6H-SiC(0001) and ≈14% with respect to GaN(0001) is huge.

In this letter, we report the growth of epitaxial, single-phase $Mn_4N(111)$ on 6H-SiC(0001) using reactive molecular-beam epitaxy (MBE). We focus on the growth, and the structural and magnetic characterization of the films. Our study shows that it is perfectly feasible to synthesize high-quality Mn_4N epitaxial films that are free from secondary phases within a large window of growth parameters.

The samples studied here are grown in a custom designed two-chamber MBE system equipped with a conventional effusion cell for Mn and an unheated NH_3 gas injector. A commercial filter purifies NH_3 and a mass-flow controller adjusts its flow into the growth chamber. 200-nm-thick Mn_4N layers are grown directly on Si-face 6H-SiC(0001) substrates at a substrate temperature of 630 °C (the temperature normally used for GaN growth is 810 °C). The NH_3 flux is adjusted to keep the chamber pressure at 8×10^{-5} Torr during growth (the pressure normally used for GaN growth is 6×10^{-6} Torr). Nucleation and growth is monitored *in situ* by reflection high-energy electron diffraction (RHEED). The structural properties of the layers are investigated by x-ray diffraction. All scans are taken with a Philips X'pert Pro™ diffractometer utilizing Cu $K\alpha_1$ radiation. For $\omega/2\theta$ scans, a 1 mm slit is used in front of the detector, while ω and ϕ scans are recorded in skew geometry with an open detector. The surface morphology of the films is examined by atomic force microscopy (AFM) and scanning electron microscopy (SEM). The magnetization measurements from 2 up to 360 K are performed in a Quantum Design superconducting quantum interference device magnetometer. Magnetization loops are recorded at various temperatures for magnetic fields between ±50 kOe. All data presented below are corrected for the diamagnetic background of the substrate.

Figures 1(a) and 1(b) show the RHEED patterns taken along the $\langle 11\bar{2}0\rangle$ azimuth of 6H-SiC at two different stages of the growth of Mn_4N. During nucleation of the layers, a spotty RHEED pattern is observed [Fig. 1(a)], which reflects

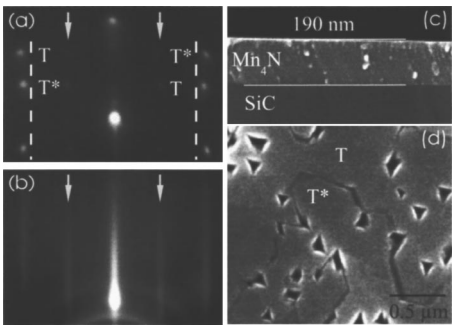

FIG. 1. RHEED patterns taken along the $\langle 11\bar{2}0\rangle$ azimuth of 6H-SiC (a) during nucleation and (b) after the deposition of 20 nm of Mn_4N. The dashed lines in (a) indicate the position of the 6H-SiC reflections, illustrating the large mismatch between these materials. Note that both (a) and (b) are displayed on a logarithmic intensity scale for better visibility. The SEM micrographs in (c) show the cross section and (d) the surface of the Mn_4N layer. T and T* in (a) and (d) refer to the rotational twins resulting from the nucleation of Mn_4N on monolayer steps of 6H-SiC.

[a]Electronic mail: dhar@pdi-berlin.de

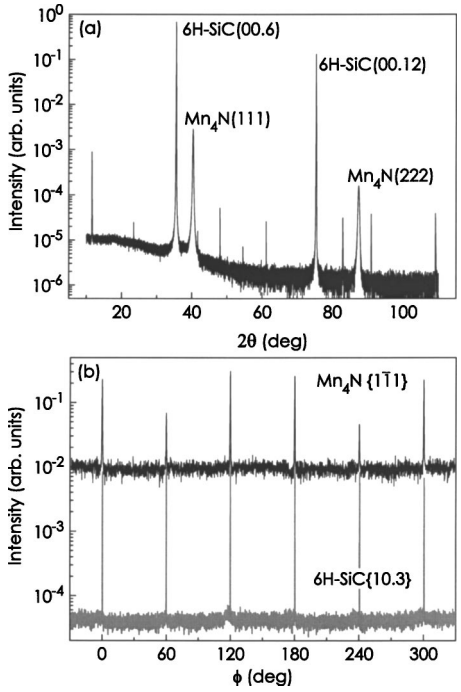

FIG. 2. (a) Symmetric x-ray $\omega/2\theta$ scan of a Mn_4N film grown on 6H-SiC(0001). (b) ϕ scans of the {10.3}-planes of 6H-SiC and the $\{1\bar{1}1\}$-planes of Mn_4N. The peaks, not labeled in (a) are due to forbidden reflections of 6H-SiC.

a three-dimensional growth mode and allows us to determine the orientation of the layer. The pattern reveals that $Mn_4N(111)\|SiC(0001)$ and the following in-plane orientation-relationship: $\langle 0\bar{1}1\rangle\|\langle 11\bar{2}0\rangle$ and $\langle 11\bar{2}\rangle\|\langle 1\bar{1}00\rangle$. Kinematical calculations of the RHEED pattern of Mn_4N show that the fundamental first-order diffraction spots (weak, marked by arrows) are due to the simple cubic N sublattice, while the (strong) second-order diffraction spots labeled T (or T^*) originate mainly from the fcc Mn sublattice. The simultaneous occurrence of both T and T^* is explained by rotational twinning, which occurs inevitably for cubic films (having trigonal symmetry) on 2H, 4H, or 6H substrates (having hexagonal symmetry) due to the different orientation of the bonds on terraces differing in height by one monolayer. Finally, by analyzing the angle of facet streaks (not shown here) we find that the initial nuclei exhibit {001} facets.

The RHEED pattern becomes streaky after the deposition of about 20 nm of Mn_4N and stays so until the end of the growth [Fig. 1(b)], reflecting two-dimensional growth. Thus, a connected film is obtained, as seen in Fig. 1(c). Figure 1(d) shows a SEM micrograph of the film's surface. The trigonal pits are seen to have an opposite orientation when comparing the areas labeled T and T^* in Fig. 1(d), thus directly visualizing the two types of domains as just discussed in relation with Fig. 1(a). These pits are likely a result of the coalescence of the initial, {001} faceted nuclei. AFM measurements of Mn_4N films of 190 nm thickness over the same 2×2 μm area as depicted in Fig. 1(d) yield values for the peak-to-valley and the rms roughness of 10–20 nm and 1–2 nm, respectively. Regions free of pits are of course significantly smoother.

Figure 2(a) shows a symmetric x-ray $\omega/2\theta$ scan taken within a wide angular range of 2θ from 10° to 110° for the film under investigation. Apart from the (00.6) and the (00.12) reflections of the substrate, the (111) [$2\theta=40.32°$] and (222) [$2\theta=87.20°$] reflections of Mn_4N can easily be identified. The remaining peaks are due to the forbidden reflections of 6H-SiC. No peak resulting from a secondary phase can be found, evidencing a high level of phase purity of this layer. Figure 2(b) compares skew geometry ϕ scans of the {10.3} planes for the 6H-SiC substrate and the $\{11\bar{1}\}$ planes for the layer. Both the substrate and the film show six equidistant maxima appearing at the same angular positions. This finding demonstrates the strict in-plane orientation relationship between the substrate and the layer. Note that the $\{1\bar{1}1\}$ planes of Mn_4N possess a threefold symmetry, while the ϕ scan of this plane exhibits six maxima. This finding reflects the double-domain nucleation of Mn_4N as just discussed in relation to Figs. 1(a) and 1(d).

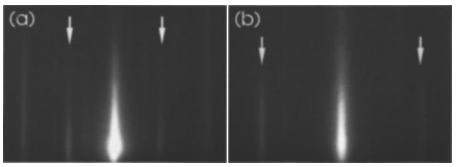

FIG. 3. RHEED patterns taken along the (a) $\langle 11\bar{2}0\rangle$ and (b) $\langle 1\bar{1}00\rangle$ azimuths of 6H-SiC at the end of the Mn_4N deposition for a sample grown at very high Mn/N flux ratio.

The crystalline quality of the films is investigated by analyzing skew geometry ω scans for the symmetric (111) and the asymmetric $(1\bar{1}1)$ reflection, which exhibit widths ranging between 0.16–0.3° and 0.25–0.39°, respectively. These values are quite comparable to those commonly observed for heteroepitaxial growth of highly mismatched materials.

In this context, it is important to mention that we have also grown Mn_4N films on GaN/6H-SiC(0001) templates. Both in terms of orientation and crystalline quality, the films are found to exhibit the same properties as those grown directly on 6H-SiC(0001) substrates. Furthermore, the results described above were found not to depend critically on growth conditions, which is surprising considering the existence of various stable Mn-N phases. In fact, we have obtained smooth single-phase Mn_4N layers for an unexpectedly wide range of conditions, namely, a substrate temperature (T_S) between 630 and 670 °C, and a Mn/N flux ratio changing over at least a factor of two.

However, we have observed that the surface quality of the films degrades as T_S is increased. At $T_S=710$ °C, the layer no longer grows as a connected film, but as isolated islands. Furthermore, at extremely high Mn/N flux ratios, the RHEED pattern exhibits fractional streaks, as depicted in Fig. 3. The position of these fractional streaks is not symmetric with respect to the first-order bulk streaks indicated by the arrows. We thus believe that these fractional streaks result from the formation of an incommensurate Mn-rich superstructure on the surface. Indeed, samples grown under these conditions exhibit an additional reflection in symmetric x-ray $\omega/2\theta$ scans at $2\theta=41.72°$, which we attribute to Mn inclusions [the angular position of this reflection coincides with that of α-Mn(114)].

Figure 4 shows the magnetization loops obtained at different temperatures for the layer of Fig. 1. The magnetization saturates at high magnetic fields and exhibits a clear hyster-

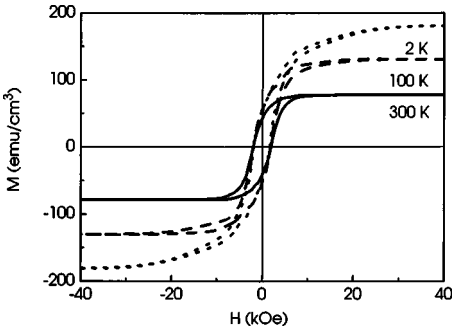

FIG. 4. Magnetization loop obtained at different temperatures. The magnetic field is applied perpendicular to the sample surface; that is, parallel to the *c* axis.

esis with a coercive field of 1700 Oe at lower fields. Furthermore, the saturation magnetization is observed to drop comparatively rapidly with temperature. These three features are consistent with the magnetic behavior of Mn_4N which is reported to exhibit ferrimagnetism with a T_N of 738 K. Indeed, the saturation magnetization per unit volume M_S measured at 2 K (178 emu/cm^3) is found to be very close to the theoretical value of 184.6 emu/cm^3 (1.15 μ_B per unit cell[8]) for Mn_4N.

To conclude, smooth Mn_4N films with a good crystalline quality can be grown either directly on SiC(0001) substrates or on GaN(0001) layers using reactive molecular-beam epitaxy. The films are found to be free from any secondary phase formation within quite a large window of growth conditions. The films shows a magnetization hysteresis above room temperature and exhibit a saturation magnetization virtually identical to the theoretical value for Mn_4N. This finding generates hopes in the direction of integrating ferromagnetic materials and wide-gap semiconductors such as SiC or GaN.

We are grateful to H. P. Schönherr and A. Bluhm for AFM and SEM scans, respectively, and thank T. Ive for his help in analyzing the AFM images and providing GaN/6H-SiC templates. Furthermore, we are indebted to L. Däweritz for critically reading of the manuscript. Part of this work has been sponsored by the Bundesministerium für Bildung and Forschung of the Federal Republic of Germany.

[1] C. M. Gürtler, Y. B. Xu, and J. A. C. Bland, J. Magn. Magn. Mater. **226–230**, 655 (2001).
[2] M. Tanaka, J. P. Harbison, T. Sands, T. L. Cheeks, V. G. Keramidas, and G. M. Rothberg, J. Vac. Sci. Technol. B **12**, 1091 (1994).
[3] K. Akeura, M. Tanaka, M. Ueki, and T. Nishinaga, Appl. Phys. Lett. **67**, 3349 (1995).
[4] W. Van Roy, H. Akinaga, S. Miyanishi, K. Tanaka, and L. H. Kuo, Appl. Phys. Lett. **69**, 711 (1996).
[5] M. Tanaka, K. Saito, and T. Nishinaga, Appl. Phys. Lett. **74**, 64 (1999).
[6] K. Inomata, K. Yusu, and Y. Saito, Phys. Rev. Lett. **74**, 1863 (1995).
[7] K. Suzuki, T. Kaneko, H. Yoshida, Y. Obi, H. Fujimori, and H. Morita, J. Alloys Compd. **306**, 66 (2000).
[8] W. J. Takei, G. Shirane, and B. C. Frazer, Phys. Rev. **119**, 122 (1960).
[9] W. J. Takei, R. R. Heikes, and G. Shirane, Phys. Rev. **125**, 1893 (1962).
[10] M. Mekata, J. Phys. Soc. Jpn. **17**, 796 (1962).
[11] S. Dhar, O. Brandt, A. Trampert, L. Däweritz, K. J. Friedland, K. H. Ploog, J. Keller, B. Beschoten, and G. Güntherodt, Appl. Phys. Lett. **82**, 2077 (2003).
[12] K. M. Ching, W. D. Chang, and T. S. Chin, Appl. Surf. Sci. **92**, 471 (1996).
[13] H. Yang, H. Al-Brithen, E. Trifan, D. C. Ingram, and A. R. Smith, J. Appl. Phys. **91**, 1053 (2002).